Reflectometry with Galileo Signals: Ocean and Amazon Basin events from CYGNSS

Dante C. Andrinolo O.
Facultad de Ingeniería,
Universidad Nacional de La Plata.
Instituto de Investigaciones en Electrónica
Control y Procesamiento de Señales - LEICI
La Plata, Buenos Aires, Argentina
dante.andrinolo@alu.ing.unlp.edu.ar

Santiago Ozafrain
Facultad de Ingeniería,
Universidad Nacional de La Plata.
Sistemas Electrónicos de Navegación
y Telecomunicaciones - SENyT
La Plata, Buenos Aires, Argentina
sozafrain@gmail.com

***Abstract*—Global Navigation Satellite Systems (GNSS) are designed to provide precise positioning, velocity, and timing information through satellite constellations. These satellites transmit signals to GNSS receivers to determine location parameters. Beyond their traditional use, GNSS signals reflected, refracted, and scattered by the Earth's surface and atmosphere have been utilized in remote sensing applications, leading to techniques like GNSS Reflectometry (GNSS-R) and GNSS Radio Occultation (GNSS-RO). GNSS-R involves processing signals reflected from the Earth's surface to extract geophysical parameters, employing GNSS-R receivers located on ground stations, airborne platforms, or Low Earth Orbit (LEO) satellites. The Cyclone Global Navigation Satellite System (CYGNSS) mission, led by the University of Michigan and sponsored by NASA, utilizes GPS-R to capture reflections of GPS L1 C/A signals. In this work we use CYGNSS public data to generate a Galileo-R event dataset, focusing on reflections from the ocean and the Amazon Basin. We processed raw intermediate frequency (IF) data to obtain Delay-Doppler Maps (DDMs) from Galileo signals, calculated relevant parameters, and created a public dataset for Galileo-R Ocean and Amazon basin events. This paper details the signal processing methodology, dataset characteristics, and a statistical analysis of the classified events.**

***Index Terms*—CYGNSS, GNSS-R, Galileo, Reflectometry, Remote Sensing.**

I. Introduction

The Global Navigation Satellite Systems (GNSS) are systems composed by satellite constellations designed to determine position, velocity and time of objects with a GNSS receiver incorporated. These satellites transmit a ranging signal that is used by the GNSS receiver to determine the localization parameters and thus, determine its own position and velocity. Besides its usual application, in the past two decades the reflected, refracted and scattered GNSS signal in the Earth's geosphere and/or atmosphere, were proposed as sources of opportunity signals for remote sensing applications, leading to GNSS Reflectometry (GNSS-R) and GNSS Radio Occultation (GNSS-RO) techniques [1], aiming to determine relevant geophysical information.

In the case of GNSS-R, the GNSS signal is reflected in the Earth surface, received and processed by a GNSS-R receiver to obtain the values of the geophysical parameters. These GNSS-R receivers can be located in a ground station or in an airborne/spaceborne platform such as a Low Earth Orbit (LEO) satellite establishing a bistatic radar geometry between the GNSS Satellites and the GNSS-R receiver as is shown in Fig. 1. The shortest signal path between the transmitter and the receiver corresponds to a reflection at the so-called specular reflection point (SP). The proposed applications of this particular technique are the estimation of wind speed [2], estimation of ice and ocean altimetry [3], [4], land humidity and temperature determination [5], [6], Cryosphere mapping [7], [8], tsunamis detection [9], and hurricane detection [10].

The usual signal processing procedure is to calculate the correlation between the reflected signal and a local replica of the characteristic quasi-orthogonal code of GNSS signals, multiplied by a carrier to compensate the Doppler effect (produced mainly by the relative movement between satellites). This is done in a frequency range where the central Doppler is expected to be. Due to poor signal-to-noise ratio (SNR) of the reflected signal, a non-coherent mean is calculated using a sequence of these correlations.This results in a bidimensional representation of the distribution of the reflected power in the delay and Doppler plane, known as Delay-Doppler Map (DDM).

The CYGNSS Mission, led by the Department of Climate and Space Sciences and Engineering in the University of Michigan and sponsored by NASA, is a GPS-R Mission that aims to calculate parameters of tropical cyclones since 2016 [10]. It is designed to capture reflections of the GPS L1 C/A civil signal, which is centered at f_c=1575.42 MHz with a $B_{W_{GPS}}$=24 MHz bandwidth, and has produced a public database of GNSS-R events with different levels of processing. This includes raw samples of the received signal and DDMs processed on-board.

Other GNSS can be used for GNSS-R, for example the Galileo system [11]. In particular, Galileo E1 civil signal shares the central frequency with GPS L1 C/A signal, with a wider bandwidth [12]. GNSS-R is an opportunistic technique that uses signals already transmitted by the navigation systems. Consequently, the location of the measured reflections depends on the GNSS constellation and the orbit of the receiver satellite. Utilizing multiple GNSS systems increases the number of

979-8-3503-6593-1/24/$31.00

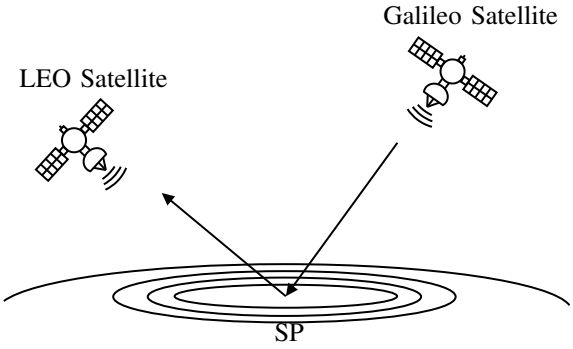

Fig. 1. Bistatic radar geometry scheme

simultaneous reflections captured, resulting in better coverage and a denser distribution of observations, making GNSS-R a more reliable technique, as it has been shown in [9], [11], [13], [14].

In this work, we generated a Galileo-R event dataset based on public data of the CYGNSS Mission. Particularly, we processed raw intermediate frequency (IF) data from CYGNSS to obtain DDMs from Galileo signals. Then, we calculated relevant parameters of these maps, such as the SP location, central Doppler frequency, SNR, among others, replicating the information provided by CYGNSS for the already processed GPS DDMs. The events were classified as 'Ocean' for reflections over the ocean surface and 'Amazon Basin' for those with signal reflections from that region. The latter is of particular interest because the drainage of the Amazon river creates ideal conditions for testing GNSS-R techniques for land moisture sensing, flood monitoring and inland water detection [15]. The dataset consists of the calculated Galileo DDM values and their associated metadata, which includes the relevant parameters mentioned above and important information for the proper usage of the data. The resulting dataset is stored in a public repository for easy access of the community with the objective to facilitate the development of GNSS-R algorithms using Galileo DDMs [16].

This article is organized as follows, in Section II we describe the geometry and the characteristics of the system, and a more detailed review of the the CYGNSS Mission's data. In Section III, the general procedure for the signal processing is outlined, such as the spatial filtering and the considerations for the procedure to be successful. We explain the characteristics of the generated dataset in this section as well. In Section IV we statistically analyze the stored events to characterize the dataset. Finally, Section V presents the conclusions of the work.

II. Reflectometry with GNSS Signals

The transmitted GNSS signal is reflected in surfaces such as ground terrain or ocean water, modifying the power and trajectories of the scattered electromagnetic waves. An appropriate description of the physical situation and characterisation of the signal have to be done to ensure a correct signal processing. In these subsections we make a brief description of the CYGNSS mission and we describe the geometry of the GNSS-R system along with the Galileo signal model and the fundamentals of GNSS-R signal processing.

A. CYGNSS Mission

The CYGNSS Mission is a GPS-R mission designed to measure ocean surface wind speed, aiming to understand the relation between surface wind and moist atmosphere within tropical cyclones, with high temporal resolution (0.5 – 1 sec) and $\sim$25 km spatial resolution [10], in operation since 2018. CYGNSS consists of a constellation of eight small LEO satellites at 510 km of altitude and 35° orbital inclination angle. Each satellite is equipped with three antennas: two nadir antennas that point across track in opposite directions to capture reflected signals, and one zenith antenna for the Line of Sight (LOS) signal. Additionally, they are equipped with a Delay Doppler Mapping Instrument (DDMI) for signal processing. Each of these instruments selects the top four captured reflections based on their localization with respect to the nadir antenna pattern. The GNSS-R processing is made every 0.5 or 1 second.

This mission has also generated a database of relevant events at different processing levels, that is available for the interested scientific public and periodically updated. This database provides, among other datasets, raw IF data in binary format of 1 minute length (most of them) of the relevant events. This dataset allows the user to apply the GNSS-R signal processing to replicate results and test new processing approaches. In addition, there is a metadata database with information about the available data such as PRN code, ID of the GPS satellite, corresponding antenna, central Doppler shifting, position coordinates of CYGNSS satellite and its roll vector, altitude, GPS time reference and other relevant information. The raw binary data also contains some of the information in the metadata: GPS weeks, GPS seconds, Local oscillator frequency of every channel, data format, and sample rate.

B. Reflected signal processing and characteristics

The Galileo Satellite and the LEO satellite (in this particular case, it belongs to the CYGNSS satellite constellation) with an incorporated GNSS-R receiver are in a bistatic radar geometry since the transmitter and the receiver are in different locations, in contrast to monostatic radar systems. Fig.1 depicts the bistatic radar geometry, where the Earth surface is the radar objective and the received signal is a reflected Galileo signal. The LOS signal is also needed during processing, as it gives information to calculate the SP location, which is necessary to estimate the Doppler shift of the reflected signal. The SP location can be calculated with an Earth model (such as WGS84) for a first approximation, using an iterative method to find the point over the surface where the angle of the incident wave is the same as the reflected one [17].

Regarding the physical qualities of the problem, the frequency and bandwidth of the Galileo signal causes the Earth's surface to generally act as a scattering surface. Thus, the

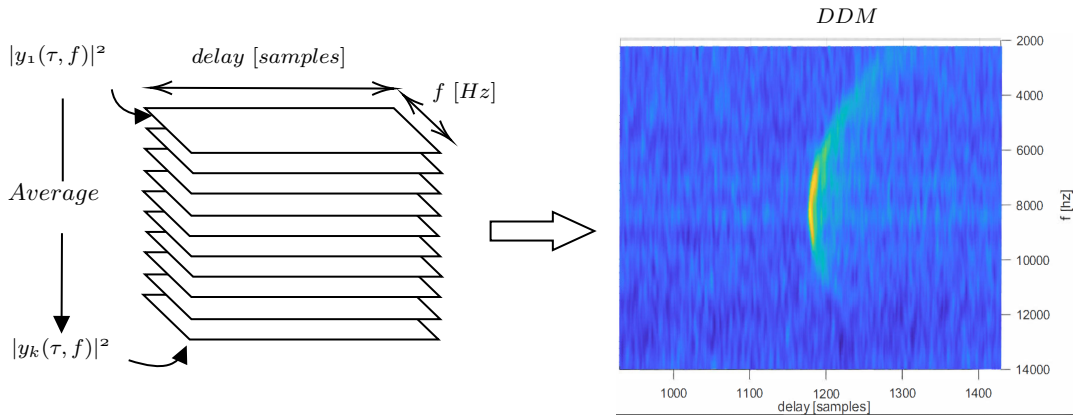

Fig. 2. Signal processing for DDM generation.

incident signal scatters in multiple directions. At LEO, the received signal arrives not only from the SP but also from surrounding points. This region, from which the scattered signal is received, is termed the "glistening zone", and its extension depends on the geometry and roughness of the surface.

The Galileo signal in the E1 band uses the same carrier frequency as GPS L1 C/A, f_c=1575.42 MHz, with a bandwidth of $B_{W_{Gal}}$=28 MHz. It employs orthogonal Pseudo Random Noise (PRN) codes to separate and identify the signals from each satellite. The PRN codes for the E1 signal have a length of 4092 and a chip rate of R_c=1023 Mchips/s, resulting in a time period of 4 ms (4 times larger than GPS). Another difference with the GPS L1 C/A is that the Galileo E1 signal uses Composite Binary Offset Carrier (CBOC) modulation that consists of a superposition of two sine Binary Offset Carrier (BOC) waveforms. This modulation broadens the bandwidth, enhancing positioning accuracy and resilience against multipath effects and interference.

The transmitted signal can be mathematically described as:

$$s(t) = d(t)c(t)b(t)\cos\left(2\pi f_c t + \theta\right) \tag{1}$$

where $d(t)$ is the data signal, f_c is the carrier frequency, $b(t)$ is the CBOC code, and $c(t)$ is the PRN code.

The signal processing consists in calculating correlations of T_i seconds between the received reflected sampled signal $r[n] = r(nT_s)$ at IF, with a local replica of the PRN code multiplied by the pertinent CBOC code and a carrier frequency aiming to compensate the Doppler shift of the reflected signal. These correlations are calculated for a specific range of delay and frequency values, centered at the estimated central Doppler shift, that can be mathematically described as:

$$y(\tau,f) = \frac{1}{\sqrt{N}}\sum_{n=1}^{N} r[n]c(nT_s-\tau)b(nT_s-\tau)e^{-j2\pi f nT_s} \tag{2}$$

where f is in the appropriate frequency range, T_s is the sample rate, $c(nT_s-\tau)$ is the sampled delayed PRN code, and N is the total number of samples in T_i seconds.

As mentioned in Section I, the DDM is obtained by non-coherently averaging consecutive correlation results, as indicated in Eq. (3). This process averages both thermal and speckle noise, which are modeled as additive and multiplicative random processes, enhancing the post-processing SNR. The non-coherent average involved in the DDM generation can be expressed as

$$Z_{DDM}(\tau,f) = \frac{1}{K}\sum_{k=1}^{K}|y_k(\tau,f)|^2 \tag{3}$$

Fig. 2 depicts a schematic representation of this procedure and a sample output DDM.

III. Galileo-R Processing

To process the raw IF data and obtain the corresponding DDMs, whether they are obtained from GPS or Galileo signals, it is necessary to know the values of some parameters that depend on the position vector and velocity vector of the GNSS and LEO satellites, such as the PRN of the reflections captured by the nadir antenna, their central Doppler and its dynamic. When processing GPS signals that information is provided in the metadata file. However, in order to process the Galileo reflected signals contained in the raw IF data register, parameters have to be calculated to obtain satisfactory DDMs. In the following section we describe this procedure.

A. Implementation details

The objective is to calculate the correlation between the received signal and the corresponding Galileo local replica with the corresponding PRN code. In first place, it is necessary to determine the useful Galileo satellite at that moment, i.e. those with a SP located within the CYGNSS antenna footprint. Since that information is not available, we perform a spatial filtering considering elevation and azimuth angles of every Galileo satellite obtained with RINEX ephemeris files for that precise date and time. Particularly, we considered Galileo-R sources with an elevation angle between 35° and 90°, filtering out those Galileo satellites below the CYGNSS LEO or with reflections with high incidence angle that are not captured by any of the nadir antennas. Additionally, we considered only

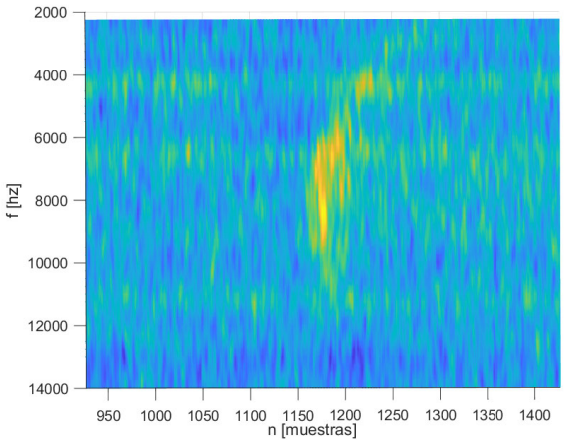

Fig. 3. Unfocused DDM caused by sample shifting.

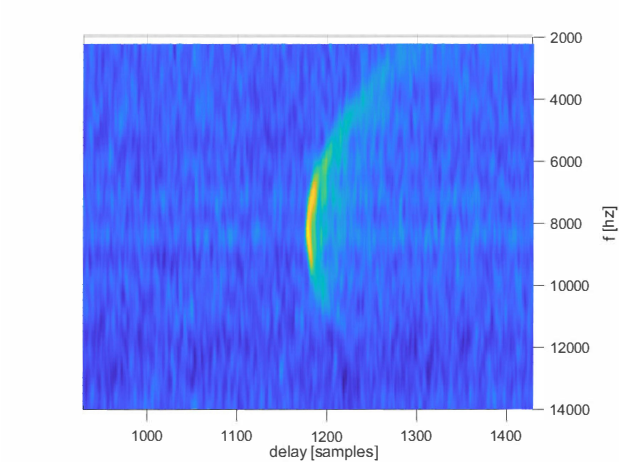

Fig. 4. Focused DDM by correcting the samples.

Galileo satellites with azimuth angles between 40° to 140° and 220° to 320°, based on the coverage pattern of the nadir antennas on both sides

Then with the position and velocity of the filtered Galileo satellites and the CYGNSS satellite (available in the Metadata file), the SP location is calculated using the WSG84 Earth model [17] and therefore the central Doppler shift is calculated following the equation (13) of [2]:

$$f_D = \frac{\vec{V}_t \cdot \vec{m} - \vec{V}_r \cdot \vec{n}}{\lambda} \tag{4}$$

where $\vec{n}$ and $\vec{m}$ are the normalized position vector of the LEO and Galileo satellites respectively considering the SP as origin, $\vec{V}_t$ and $\vec{V}_r$ are the velocity vectors of the Galileo and CYGNSS satellites.

Then, the correlation is computed following Eq. (2) using T_i=4 ms, which indicates one PRN code period, with a Doppler range of ±6 kHz centered at the estimated SP Doppler shift and a step of 250 Hz between frequency bins. The DDMs are calculated with the non-coherent average from Eq. (3), using K=250 to obtain a 1 second DDM. Then, for each file we obtain sequences of consecutive DDMs from all the selected Galileo satellites, with a time resolution of 1 second spanning the total duration of the register.

Regarding the consecutive calculation of the correlation maps a sample correction is needed, particularly because of two effects: i) the sampling frequency of the IF signal is not coherent with the chip rate and ii) the Doppler shifting effect of the code. The raw IF data is sampled at f_s=16.0362 MHz. For Ti=4 ms, we obtain $N = f_s T_i$ =64144.8, which is not an integer, so we use $N = 64144$. The difference of 0.8 samples accumulates a delay error that, if not compensated, leads to a shift in the received signal's delay for each correlation. In consequence, the DDMs become 'unfocused', and the SNR degrades as shown in Fig. 3. Additionally, due to the Doppler frequency shift, the received code's chip rate is altered, generating a shift between local code's chip and received code's chip and thus increasing the misalignment of consecutive correlations in the DDMs [18]. To ensure proper processing, we compensate for both errors in each correlation by shifting the local replica once the error accumulates to over one sample. For the previous example, the corrected DDM is shown in Fig. 4.

B. Dataset structure

From all the Galileo-R events captured in the CYGNSS Raw IF data registers we classified those with an SP located at the ocean as 'Ocean' and those at the Amazon Basin as 'Amazon Basin'. Then these events were processed following the previously explained pipeline. The DDMs and calculated parameters were saved on a netCDF file and are available to the public. The saved data is shown in Table I.

IV. Statistical Analysis of the Dataset

Of the 477 raw IF data registers available in the CYGNSS database, 56 were classified as 'Ocean' or 'Amazon basin' and suitable for processing. The dataset is composed of 26 'Ocean' events and 30 'Amazon Basin' events.

Table II shows the results of the statistical analysis of the data. Regarding the Ocean cases, considering an SNR higher to 0 dB as useful, the mean useful time per event, is 22.67 seconds, and the mean SNR computed as $10\log_{10}(\overline{\text{SNR}})$ (where $\overline{\text{SNR}}$ is the mean SNR in linear scale) is 7.8 dB and the mean elevation angle is 56.72°. Analyzing the SNR histogram in Fig. 5, which was computed for every DDM with a SNR greater than -3 dB to avoid an SP outside the antenna footprint (let us call it 'healthy DDMs'), it can be showed that 90% of the useful cases has an SNR between 0 and 15.1dB. For the useful time, the histogram in Fig. 6 shows a distribution with a peak at 0-5 seconds and a mostly uniform distribution at 20-45 seconds with a peak at 60 seconds, which is the maximum length of the registers. In the case of the elevation angle, the majority of cases the elevation angle relies from 45° to 55° with a peak of cases at 75° (Fig. 7).

Regarding the 'Amazon basin' classified events, the mean SNR is 8.52dB, the mean useful time is 25.5 seconds per register, and the mean elevation angle is 53°. In comparison to the

TABLE I
NETCDF SAVED DATA

DDM data	Galileo-R Event data
DDM	Start date
SNR [dB]	End date
Central Doppler	DDM timestamp
Galileo position (ECEF)	DDM gps week
Galileo velocity (ECEF)	DDM gps second
CYGNSS satellite position (ECEF)	CYGNSS satellite roll
CYGNSS satellite velocity (ECEF)	CYGNSS satellite yaw
SP position (ECEF)	CYGNSS satellite pitch
PRN Code	CYGNSS satellite latitude
Antenna	CYGNSS satellite longitude
Frequency range	CYGNSS satellite altitude
Chip range	

TABLE II
SUMMARY OF THE DATA STATISTICS FOR EACH CLASSIFICATION

	Ocean	Amazon basin
Mean useful time [sec]	22.67	25.5
Mean SNR [dB]	7.8	8.52
Mean elevation angle [degrees]	56.72	53

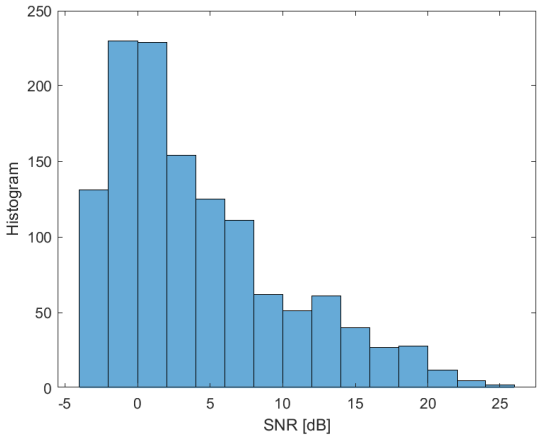

Fig. 5. SNR histogram for 'Ocean' classified events.

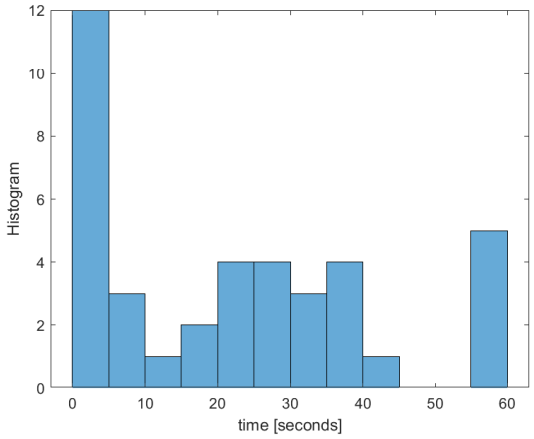

Fig. 6. Useful register time histogram for 'Ocean' classified events.

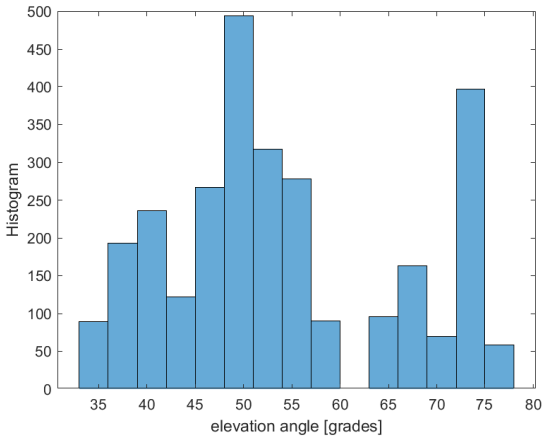

Fig. 7. Elevation angle histogram for 'Ocean' classified events.

Ocean case as shown in Fig. 8, 90% of the cases has an SNR between 0 and 15.8dB, which is greater due to the reflection on the ground. It should also be noted that the Amazon basin SNR histogram has more events for greater SNR, reaching 25dB in comparison to the ocean case. In the case of the useful register time a bigger proportion relies between 0 and 20 seconds with a peak on 60 seconds as shown in Fig. 9. Finally, regarding the elevation angle, 40° to 60° represent the majority of the cases (Fig. 10), while in comparison to the Ocean cases, there are few cases at 70° elevation angle. These histograms show that the processing implemented for the Galileo DDMs achieved satisfactory results with the CYGNSS raw IF data in generating a useful dataset of GNSS-R events.

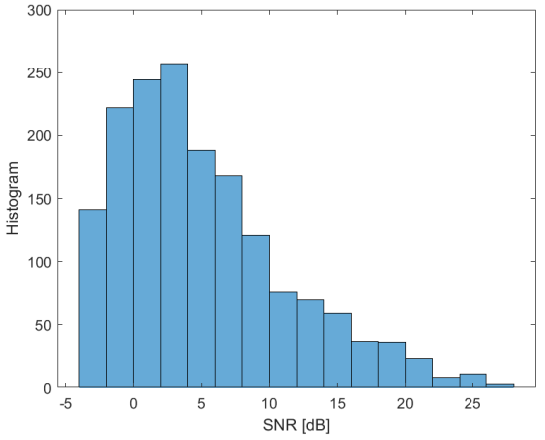

Fig. 8. SNR histogram for 'Amazon basin' classified events.

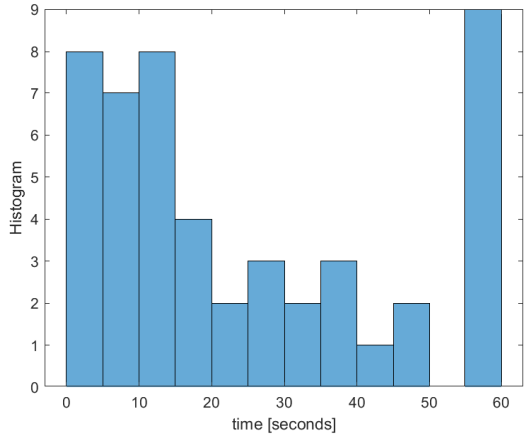

Fig. 9. Useful register time histogram for 'Amazon basin' classified events.

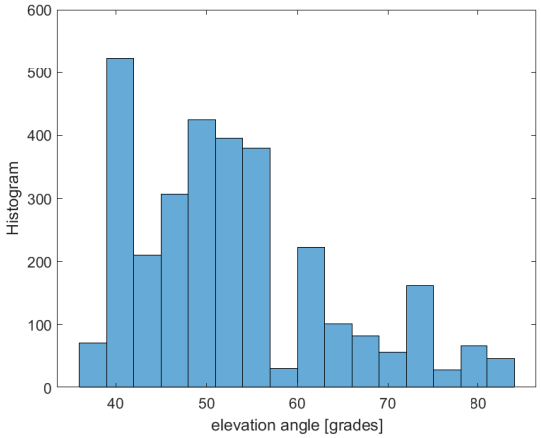

Fig. 10. Elevation angle histogram for 'Amazon basin' classified events.

V. Conclusions

In this work we have generated a Galileo Reflectometry dataset for signal reflected over the ocean surface and the Amazon Basin, based on CYGNSS mission database. Using the CYGNSS satellites position, we have computed a spatial filter to determine possible Galileo-R sources. The usual GNSS-R signal processing procedure was adapted to the Galileo signal. A total of 56 Galileo-R events classified as 'Amazon basin' and 'Ocean' were processed, and finally we made a statistical analysis of relevant parameters of the computed data. This analysis shows a great amount of useful DDMs with a good useful time of duration for the proposed classification. This dataset which can be downloaded from [16] could be very helpful for research aiming to employ Galileo-R o multi-system schemes of GNSS-R.

As future work this pipeline can be used to extend the dataset for different type of Galileo-R events or for new Ocean and Amazon basin events. In addition, the signal processing can be modified to calculate DDMs using personalized criteria for different Galileo-R applications in future projects.

References

[1] S. Jin, E. Cardellach, and F. Xie, *GNSS Remote Sensing: Theory, Methods and Applications*. Springer Netherlands, 2014. [Online]. Available: http://dx.doi.org/10.1007/978-94-007-7482-7

[2] V. Zavorotny and A. Voronovich, "Scattering of GPS signals from the ocean with wind remote sensing application," *IEEE Transactions on Geoscience and Remote Sensing*, vol. 38, no. 2, p. 951–964, Mar. 2000. [Online]. Available: http://dx.doi.org/10.1109/36.841977

[3] S. T. Lowe, C. Zuffada, Y. Chao, P. Kroger, L. E. Young, and J. L. LaBrecque, "5-cm-Precision aircraft ocean altimetry using GPS reflections," *Geophysical Research Letters*, vol. 29, no. 10, pp. 13–1–13–4, 2002. [Online]. Available: https://agupubs.onlinelibrary.wiley.com/doi/abs/10.1029/2002GL014759

[4] G. Ruffini, F. Soulat, M. Caparrini, O. Germain, and M. Martín-Neira, "The Eddy Experiment: Accurate GNSS-R ocean altimetry from low altitude aircraft," *Geophysical Research Letters*, vol. 31, no. 12, 2004. [Online]. Available: https://agupubs.onlinelibrary.wiley.com/doi/abs/10.1029/2004GL019994

[5] M. P. Clarizia, N. Pierdicca, and F. Costantini, "Analysis of CYGNSS Data for Soil Moisture Applications," in *IGARSS 2018 - 2018 IEEE International Geoscience and Remote Sensing Symposium*, 2018, pp. 1411–1413.

[6] A. Calabia, I. Molina, and S. Jin, "Soil Moisture Content from GNSS Reflectometry Using Dielectric Permittivity from Fresnel Reflection Coefficients," *Remote Sensing*, vol. 12, no. 1, 2020. [Online]. Available: https://www.mdpi.com/2072-4292/12/1/122

[7] A. Alonso-Arroyo, V. U. Zavorotny, and A. Camps, "Sea Ice Detection Using U.K. TDS-1 GNSS-R Data," *IEEE Transactions on Geoscience and Remote Sensing*, vol. 55, no. 9, pp. 4989–5001, 2017.

[8] Y. Zhu, T. Tao, K. Yu, Z. Li, X. Qu, Z. Ye, J. Geng, J. Zou, M. Semmling, and J. Wickert, "Sensing Sea Ice Based on Doppler Spread Analysis of Spaceborne GNSS-R Data," *IEEE Journal of Selected Topics in Applied Earth Observations and Remote Sensing*, vol. 13, pp. 217–226, 2020.

[9] R. Stosius, G. Beyerle, A. Hoechner, J. Wickert, and J. Lauterjung, "The impact on tsunami detection from space using GNSS-reflectometry when combining GPS with GLONASS and Galileo," *Advances in Space Research*, vol. 47, no. 5, pp. 843–853, 2011, scientific applications of Galileo and other Global Navigation Satellite Systems - II. [Online]. Available: https://www.sciencedirect.com/science/article/pii/S0273117710006393

[10] C. S. Ruf, R. Atlas, P. S. Chang, M. P. Clarizia, J. L. Garrison, S. Gleason, S. J. Katzberg, Z. Jelenak, J. T. Johnson, S. J. Majumdar, A. O'brien, D. J. Posselt, A. J. Ridley, R. J. Rose, and V. U. Zavorotny, ""New Ocean Winds Satellite Mission to Probe Hurricanes and Tropical Convection"," *Bulletin of the American Meteorological Society*, vol. 97, no. 3, pp. 385 – 395, 2016. [Online]. Available: https://journals.ametsoc.org/view/journals/bams/97/3/bams-d-14-00218.1.xml

[11] F. Gao, T. Xu, N. Wang, C. Jiang, Y. Du, W. Nie, and G. Xu, "Spatiotemporal Evaluation of GNSS-R Based on Future Fully Operational Global Multi-GNSS and Eight-LEO Constellations," *Remote Sensing*, vol. 10, no. 1, 2018. [Online]. Available: https://www.mdpi.com/2072-4292/10/1/67

[12] European Space Agency, *European GNSS (Galileo) Open Service Signal In Space Interface Control Document (OS SIS ICD), Issue 2.0*, 2nd ed., European Space Agency, January 2021.

[13] H. Carreno-Luengo and A. Camps, "First Dual-Band Multiconstellation GNSS-R Scatterometry Experiment Over Boreal Forests From a Stratospheric Balloon," *IEEE Journal of Selected Topics in Applied Earth Observations and Remote Sensing*, vol. 9, no. 10, pp. 4743–4751, 2016.

[14] M. L. Hammond, G. Foti, J. Rawlinson, C. Gommenginger, M. Srokosz, L. King, M. Unwin, and J. Roselló, "First Assessment of Geophysical Sensitivities from Spaceborne Galileo and BeiDou GNSS-Reflectometry Data Collected by the UK TechDemoSat-1 Mission," *Remote Sensing*, vol. 12, no. 18, 2020. [Online]. Available: https://www.mdpi.com/2072-4292/12/18/2927

[15] P. T. Setti and S. Tabibi, "Spaceborne GNSS-Reflectometry for Surface Water Mapping in the Amazon Basin," *IEEE Journal of Selected Topics in Applied Earth Observations and Remote Sensing*, vol. 17, pp. 6658–6670, 2024.

[16] D. Andrinolo and S. Ozafrain, "Reflectometry with Galileo Signals: Ocean and Amazon Basin events from CYGNSS," Jun. 2024. [Online]. Available: https://doi.org/10.5281/zenodo.11660186

[17] D. J. G. Sanz Lucas, Scillone German, “Radio Ocultación y Reflectometría GNSS en satélites de órbita baja. Trabajo final de grado para la carrera de Ingeniería Electrónica en Facultad de Ingeniería,” 2021.

[18] Kaplan, E.D. and Hegarty, C.J., *Understanding GPS: Principles and Applications*, ser. Artech House mobile communications series. Artech House, 2006.